Atmos. Meas. Tech., 5, 1085–1098, 2012
www.atmos-meas-tech.net/5/1085/2012/
doi:10.5194/amt-5-1085-2012

Atmospheric Measurement Techniques

Ship emissions of SO_2 and NO_2: DOAS measurements from airborne platforms

N. Berg[1], **J. Mellqvist**[1], **J.-P. Jalkanen**[2], **and J. Balzani**[3]

[1]Chalmers University of Technology, Göteborg, Sweden
[2]Finnish Meteorological Institute, Helsinki, Finland
[3]Joint Research Centre, Ispra, Italy

Correspondence to: J. Mellqvist (johan.mellqvist@chalmers.se)

Received: 18 May 2011 – Published in Atmos. Meas. Tech. Discuss.: 11 October 2011
Revised: 8 March 2012 – Accepted: 30 March 2012 – Published: 15 May 2012

Abstract. A unique methodology to measure gas fluxes of SO_2 and NO_2 from ships using optical remote sensing is described and demonstrated in a feasibility study. The measurement system is based on Differential Optical Absorption Spectroscopy using reflected skylight from the water surface as light source. A grating spectrometer records spectra around 311 nm and 440 nm, respectively, with the telescope pointed downward at a 30° angle from the horizon. The mass column values of SO_2 and NO_2 are retrieved from each spectrum and integrated across the plume. A simple geometric approximation is used to calculate the optical path. To obtain the total emission in $kg\,h^{-1}$ the resulting total mass across the plume is multiplied with the apparent wind, i.e. a dilution factor corresponding to the vector between the wind and the ship speed. The system was tested in two feasibility studies in the Baltic Sea and Kattegat, from a CASA-212 airplane in 2008 and in the North Sea outside Rotterdam from a Dauphin helicopter in an EU campaign in 2009. In the Baltic Sea the average SO_2 emission out of 22 ships was $(54 \pm 13)\,kg\,h^{-1}$, and the average NO_2 emission was $(33 \pm 8)\,kg\,h^{-1}$, out of 13 ships. In the North Sea the average SO_2 emission out of 21 ships was $(42 \pm 11)\,kg\,h^{-1}$, NO_2 was not measured here. The detection limit of the system made it possible to detect SO_2 in the ship plumes in 60 % of the measurements when the described method was used.

A comparison exercise was carried out by conducting airborne optical measurements on a passenger ferry in parallel with onboard measurements. The comparison shows agreement of (-30 ± 14) % and (-41 ± 11) %, respectively, for two days, with equal measurement precision of about 20 %. This gives an idea of the measurement uncertainty caused by errors in the simple geometric approximation for the optical light path neglecting scattering of the light in ocean waves and direct and multiple scattering in the exhaust plume under various conditions. A tentative error budget indicates uncertainties within 30–45 % but for a reliable error analysis the optical light path needs to be modelled.

A ship emission model, FMI-STEAM, has been compared to the optical measurements showing an 18 % overestimation and a correlation coefficient (R^2) of 0.6. It is shown that a combination of the optical method with modelled power consumption can estimate the sulphur fuel content within 40 %, which would be sufficient to detect the difference between ships running at 1 % and at 0.1 %, limits applicable within the IMO regulated areas.

1 Introduction

The emission of sulphur can damage human health and contribute to acidification, damaging sensitive ecosystems. The emission of NO_x contributes to acidification and formation of ground level ozone which can in turn harm human health and vegetation (Corbett et al., 2007). Modelling studies have shown that emissions from shipping contribute significantly to acid rain in many parts of Europe (Johnson et al., 2000). Ships are major sources of atmospheric pollutants; in Europe, emissions of SO_2 and NO_x from shipping are projected to exceed all the land-based emissions by 2020 (European Commission, 2005). Before 2005 the shipping sector had no regulations on emissions of sulphur, NO_x and particulate matter. Large ship emissions have now been acknowledged by the

International Maritime Organization (IMO) as an important issue and SO_x and NO_x emissions from ship exhausts are now regulated in the International Convention for the Prevention of Pollution from Ships (MARPOL) Annex VI. In special Emission Control Areas (ECA) more stringent standards are set. The Baltic Sea and North Sea are SO_x ECAs, in effect from 19 May 2006 and 22 November 2007 respectively. From 1 August 2012, North America will be both a NO_x and SO_x ECA, (IMO, 2009).

Since there is a considerable price difference between high and low sulphur fuel there is economic incentive to contravene the legislation and use cheaper residual fuel containing high concentrations of sulphur.

In this study an optical system has been developed based on the recording of skylight reflected on the water surface to estimate total emissions of SO_2 and NO_2 from ships. The overall approach is unique, to our knowledge, although the method is based on the DOAS (Differential Optical Absorption Spectroscopy) technique (Platt et al., 1979) which has been used in various applications over the last 30 yr. This includes long path measurements of pollutants (Yu et al., 2008), ground based multi-axis DOAS measurements of skylight to retrieve volcanic gas fluxes of SO_2 (Galle et al., 2003) and mobile zenith sky measurements of gas fluxes from industrial conglomerates (Rivera et al., 2009). The DOAS technique is also operated from numerous satellite sounders measuring reflected solar light from the earth surface. For instance the instruments SCIAMACHY (Lee et al., 2008) and GOME measuring both SO_2 and NO_2 among other species. The NO_2 measurements from the GOME instrument (Beirle et al., 2004) shows enhanced NO_2 along the shipway tracks in the Indian Ocean,. The DOAS technique has also been used from airplanes; Wang et al. (2006) for instance carried out airborne SO_2 measurements of combustion plants in the Po valley recording ultraviolet light reflected from the ground. The manner the gas flux is derived from the optical measurements here is similar to other mobile remote sensing applications carried out from the ground (Mellqvist et al., 2010; Rivera et al., 2009) i.e. multiplying the measured mass across the plume with the wind speed.

The optical system described here has been developed as part of a national project named IGPS (Identification of Gross Polluting Ships), aimed at developing a surveillance system to control whether individual ships obey the IMO legislation of reduced sulphur fuel content (SFC) and NOx emissions, as discussed above. The optical system is here combined with an in situ system (Mellqvist and Berg, 2012) that measures ratios of the pollutants against CO_2, and from this the SFC and NO_x emission per fuel unit is directly derived (Williams et al., 2009). The disadvantage with the in situ system is that it requires flying directly into the ship plume, at low altitude 50 to 150 m, and the fact that only relative emissions are obtained. To improve this, the optical system will be used as a first alert system that will indicate whether a ship is disobeying the IMO legislation and this may trigger low level flying in the plume with the in situ system.

In the following chapters the hardware, measurement methodology and test measurements in both helicopter and airplane will be described. The acquired data have been compared to a ship model calculation.

2 Experimental

2.1 Hardware

The optical system consists of a single UV spectrometer (Andor Shamrock 303i spectrometer, 303 mm focal length, variable slit – set to 500 µm) equipped with a CCD detector (Andor Newton DU920N-BU2, 1024 by 255 pixels, thermoelectrically cooled to $-70\,^{\circ}C$). The wavelength region and resolution of the spectrometer can be controlled automatically by choosing one out of three gratings which are installed in a turret. The switch time between the gratings is a few seconds. In this study two wavelength region have been applied, i.e. 294 and 324 nm for SO_2 with a spectral resolution of 0.71 nm (2400 grooves/mm grating) and 420 to 459 nm for NO_2 with a resolution of 0.97 nm (holographic grating of 1800 grooves/mm). The choice of spectral resolution was originally chosen to be 30 % higher, using a 300 µm slit width, but due to a malfunctioning slit controller the used slit width became higher than intended, i.e. 500 µm.

The spectrometer is connected to a quartz telescope (focal length 150 mm, lens diameter 75 mm) through a liquid light guide, diameter 3 mm, yielding a field of view of 20 mrad. Two optical band pass filters (Hoya and a custom made one from Layertec) are used inside the telescope in front of the light guide entrance to prevent stray light in the spectrometer, by blocking wavelengths longer than 325 nm. These filters are only used when measuring SO_2.

The spectrometer accumulates spectra with a cycle time of one second. The exposure time is dependent on the amount of reflected skylight on the water surface. The longest exposure time is one second and typically 5–20 spectra are accumulated each second.

2.2 DOAS methodology

The evaluation procedure is carried out using the DOAS approach proposed by Platt et al. (1979) utilizing differential features of the molecular absorption. There are some variants how to carry out the retrieval and here we have first high pass filtered the measured spectra (differential spectra) and the cross sections for each species. For each measurement run, transecting a ship plume, the first spectrum is taken as a sky reference which is used to eliminate the absorption features of the atmosphere.

In the spectral retrieval the differential absorption cross-sections for the selected species, the logarithm of the differential sky reference spectrum and ring spectrum are scaled

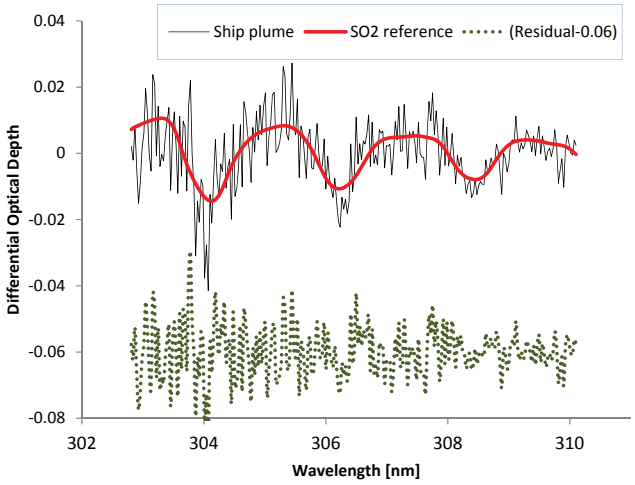

Fig. 1. A ship plume measurement of SO_2 corresponding to the plume in Fig. 7. The differential optical depth is shown when normalizing spectra inside and outside the ship plume, respectively, and correcting for the ring spectrum. In addition a fitted reference spectrum of SO_2 is shown. The lower part shows the residual after the fitting procedure.

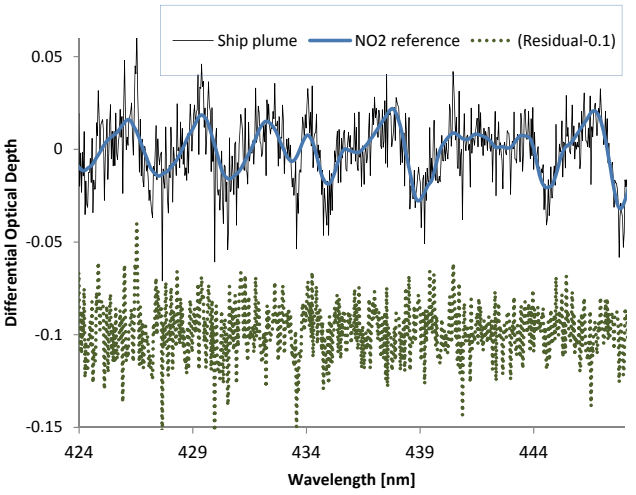

Fig. 2. A ship plume measurement of NO_2 corresponding to the last plume in Fig. 6. The differential optical depth is shown when normalizing spectra inside and outside the ship plume, respectively, and correcting for the ring spectrum. In addition a fitted reference spectrum of NO_2 is shown. The lower part shows the residual after the fitting procedure.

to the logarithm of the measured differential spectra by multivariate fitting using the DOASIS software package (Kraus, 2006). The ring spectrum corresponds to spectral structures coming from inelastic atmospheric scattering (Grainger and Ring, 1962; Fish and Jones, 1995). The spectrum has been obtained through the DOASIS software which calculates a ring spectrum from the Raman scattering processes of atmospheric nitrogen and oxygen applied to the intensities of the reference spectrum.

The absorption cross-sections used for SO_2 and NO_2 were obtained from Vandaele et al. (1998), adapted to our instrument by the software WinDOAS (Van Roozendael and Fayt, 2001). This is done by convoluting the absorption cross-section with the instrument function of the spectrometer, obtained from a low pressure Hg lamp measurement.

Examples of spectral fits for SO_2 and NO_2 are shown in Figs. 1 and 2, respectively, showing measurements inside ship plumes for the data in Figs. 6 and 7. In the SO_2 evaluation region the residual noise increases progressively towards the shorter wavelengths due to diminishing light.

The SO_2 columns in the spectra was retrieved in the spectral region 302 to 310 nm by fitting the differential absorption cross section of SO_2 and a ring spectrum. The interfering species ozone was omitted from the retrieval to minimize the degrees of freedom in the fitting procedure for improved baseline stability in the column measurement. This has no significant effect on the results. Note that the plume is only intercepted during a few seconds and since the time difference between the plume and reference measurements is very short there will be no change in the background atmospheric column of ozone.

The column of NO_2 was retrieved in the spectral region 424 to 448 nm by fitting the differential absorption cross section of NO_2 and a ring spectrum. We have omitted water as an interfering species for the same reason as ozone above.

3 Methodology

3.1 Measurement methodology

The emission measurements are carried out by conducting flight transects above and perpendicular to the exhaust plume of the ships. This is illustrated in Fig. 3, for an actual measurement that was carried out in the project.

An approach with multiple turns towards the ship provides the possibility of measuring the emissions several times without interference from the aircraft exhaust. The optimal flight path which we tried to achieve in the measurements is illustrated in Fig. 4. The ship plume direction is determined by the apparent wind, which is the resultant wind of the true wind and the wind created by the ship velocity and heading. This apparent wind is the wind felt standing on the ship. Spectra are recorded with the telescope pointed downwards at a 30° angle from the horizon and 90° angle relative to the aircraft heading. The reason for the chosen telescope angle of 30° below the horizon is the fact that sea surface reflectance increases strongly with the incidence angle, (Fresnel equation) and the angle used is a good compromise between the distance to the ship (optical path of light) and the intensity.

In the light path estimation it is assumed that the skylight is specularly reflected on the ocean surface at a slant angle

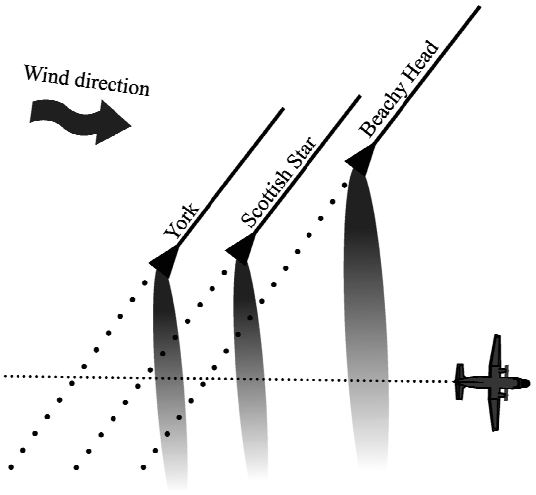

Fig. 3. An illustration of a flight transect across emission plumes from the ships Jork, Scottish Star and Beachy Head. The ships were travelling northwards in the Baltic Sea, outside the island of Gotland. The measurement was carried out from a CASA-212, an airplane operated by the Swedish coastguard on 24 August 2009. The corresponding raw data of NO_2 is shown in Fig. 6.

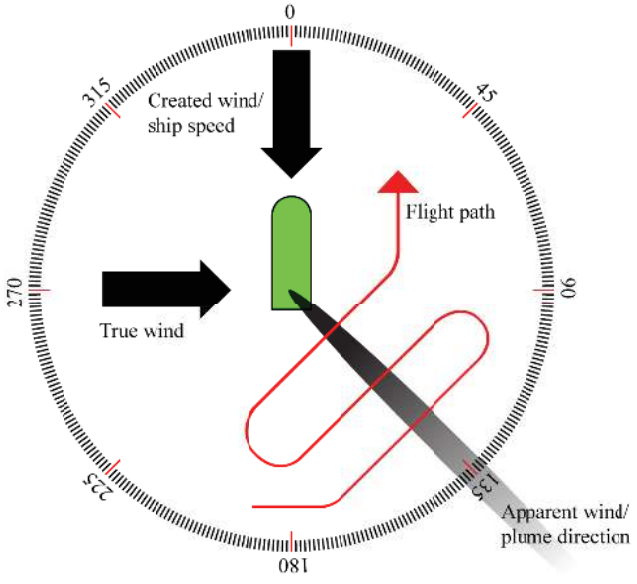

Fig. 4. Illustration of the desired flight path across the plume for the optical measurements. The ship plume points in the direction of the apparent wind which corresponds to the resulting wind of the ship speed and heading and the true wind.

of 30° corresponding to the telescope angle. The light hence passes twice through the gas plume. In Fig. 5 an illustration of the light path through the plume is shown. The grey area in the figure illustrates the fact that waves will influence the optical light path of the observed skylight and hence cause an uncertainty in the angle by which the light passes through the gas plume. This is further discussed in Sect. 6 together with

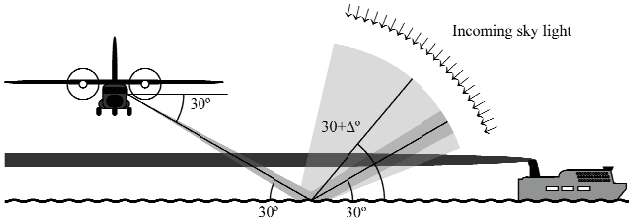

Fig. 5. Illustration of the airborne optical measurement of the ship emissions. It is assumed that the skylight is specularly reflected on the ocean surface at a slant angle of 30° corresponding to the telescope angle and the light hence passes twice through the gas plume. The presence of waves widens the field of view observed and causes an uncertainty in the angle by which the light passes through the gas plume.

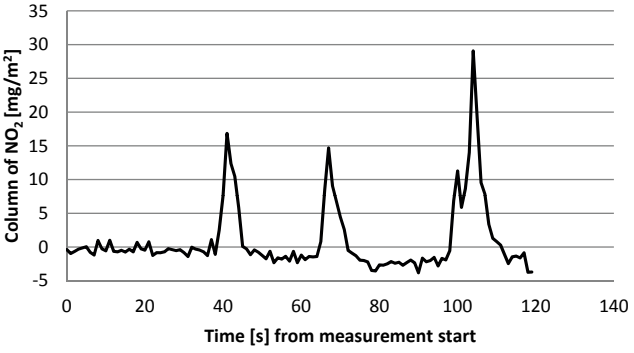

Fig. 6. Optical measurement of NO_2 for the flight transect illustrated in Fig. 3. The standard deviation of the background is $0.44\,\mathrm{mg\,m^{-2}}$.

an additional uncertainty regarding light scattering directly in the plume.

In Fig. 6 an optical measurement of NO_2 is shown when conducting a flight transect across three ships in the Baltic Sea, as illustrated in Fig. 3. The measurement is well above the noise, which here corresponds to a 1-σ level of $0.44\,\mathrm{mg\,m^{-2}}$. A corresponding measurement of SO_2 is shown in Fig. 7 for a large passenger ferry measured outside Rotterdam harbour, with a 1-σ noise level of $2.7\,\mathrm{mg\,m^{-2}}$.

3.2 Emission calculation

The ship emissions are calculated by integrating the column values of the peak over the fitted baseline multiplied with the apparent wind. The values are compensated for the flight direction relative to the plume and the telescope viewing angle (Eq. 1).

$$\text{flux} = \sum \text{mass Column} \cdot L \cdot v_{\mathrm{AW}} \cdot k_{\mathrm{ortho}} \cdot k_{\mathrm{airmass}}. \quad (1)$$

In Eq. (1) the mass column is given by the spectroscopic measurement. The accumulated cycle time for each spectrum (typically 1s) combined with the aircraft velocity gives the distance, L, along the flight transect of the gas to which

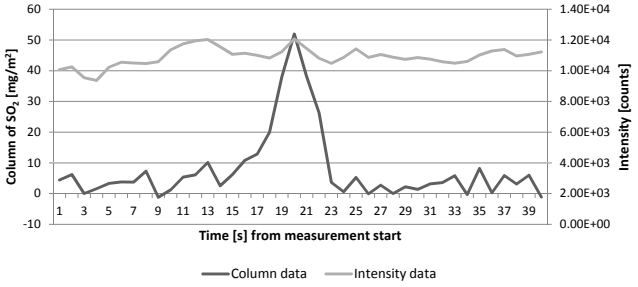

Fig. 7. Optical measurement of SO_2 for a flight transect across the plume of a large ferry outside Rotterdam harbour on 25 September 2009 at 15:00 LT (local time). The noise level is 2.7 mg m^2. The intensity at 311 nm is shown.

each gas column corresponds. The apparent wind, illustrated in Fig. 4 is the resultant wind speed (v_{AW}) and wind direction (θ_{AW}) of the plume, as calculated by Eqs. (2)–(4) using the ship and true wind speed and heading. The atan2 expression in Eq. (3) is a generally available variation of the arctangent function which returns the inverse tangent of the first (x) and second (y) argument to the function. The apparent wind velocity is used directly in the flux calculation and the apparent wind direction is used when compensating for non-orthogonal flight transects across the plume by the factor k_{ortho} in Eq. (5).

$$v_{\mathrm{AW}} = \sqrt{\left(\mathrm{ship}_{\mathrm{vel.\ east}} + \mathrm{wind}_{\mathrm{vel.\ east}}\right)^2 + \left(\mathrm{ship}_{\mathrm{vel.\ north}} + \mathrm{wind}_{\mathrm{vel.\ north}}\right)^2} \quad (2)$$

$$\theta_{\mathrm{AW}} = -\mathrm{atan2}\left[\left(\mathrm{ship}_{\mathrm{vel.\ east}} + \mathrm{wind}_{\mathrm{vel.\ east}}\right), \left(\mathrm{ship}_{\mathrm{vel.\ north}} + \mathrm{wind}_{\mathrm{vel.\ north}}\right)\right] \quad (3)$$

$$\left\{\begin{array}{l} \mathrm{ship}_{\mathrm{vel.\ north}} = v_{\mathrm{ship}} \cdot \cos\left(-\theta_{\mathrm{ship}} + \pi\right) \\ \mathrm{ship}_{\mathrm{vel.\ east}} = v_{\mathrm{ship}} \cdot \sin\left(-\theta_{\mathrm{ship}} + \pi\right) \\ \mathrm{wind}_{\mathrm{vel.\ north}} = v_{\mathrm{wind}} \cdot \cos\left(-\theta_{\mathrm{wind}} + \pi\right) \\ \mathrm{wind}_{\mathrm{vel.\ east}} = v_{\mathrm{wind}} \cdot \sin\left(-\theta_{\mathrm{wind}} + \pi\right) \end{array}\right\} \quad (4)$$

$$k_{\mathrm{ortho}} = \left|\sin\left(\theta_{\mathrm{travel}} - \theta_{\mathrm{AW}}\right)\right|. \quad (5)$$

The airmass factor k_{airmass} is a geometric approximation of the AMF which corresponds to $1/2 \cdot \sin(\theta_{\mathrm{telescope}})$ and it corrects for the slant angle of the light assuming a double light passage through the plume with the telescope angle $\theta_{\mathrm{telescope}}$ (typically 30°) and a flat ocean. This approximation becomes uncertain in the presence of waves and other error sources which is further discussed in Sect. 6.1. In the emission calculation we have also assumed the flight speed to be significantly higher than the wind speed, neglecting the fact that the plume moves in the same direction as the aircraft, this is instead taken into account in the error estimation.

4 Measurements

The optical system presented here has been used in two measurement campaigns, carried out along the coast of Sweden, mainly in the Baltic Sea, and the North Sea between Oostende and Rotterdam. A CASA-212 airplane was used in the Baltic Sea campaign operated by the Swedish Coast Guard. During the test flights the crew consisted of two pilots and one surveillance systems operator. The measurement flights were carried out on 7 days between 12 and 24 August 2008 using Visby airfield as base, which provides quick access to the larger shipping routes in the Baltic Sea. The on board surveillance system was used to document ship information, such as name, IMO number speed and heading. Other ship parameters, such as dead weight (DWT), date of build (DOB) and ship type, were later collected from a web database (http://www.vesseltracker.com/). The CASA-212 flight system provided airplane speed, heading and altitude and also wind speed and direction by comparing the true movement relative to ground to the heading of the aircraft and measured airspeed. The wind measurements were made at the altitude of the plume and compared with station data from the island of Gotland; often the average daily wind speed was used but also individual wind measurements of the ships. The spectrometer was located in the cargo bay of the aircraft connected to the telescope using a liquid light guide. The telescope was mounted on a tripod standing inside of the rear entry door, which had a bulb window that could be opened during flight. The flight speed during measurements was 110 to 160 knots (i.e. 55–80 m s^{-1}) and the altitude varied between 350 and 1000 feet, mainly 950 feet (290 m).

The second campaign was undertaken in the North Sea in the vicinity of Rotterdam as part of the SIRENAS-R campaign, a study financed by the DG Environment- Clean Air and Transport, through the Joint Research Centre in ISPRA and the Belgian DG environment. The measurements were carried out with a Dauphin helicopter, operated by Noordzee Helikopters Vlaanderen. The crew consistsed of two pilots and one hoist operator. Measurements flights were performed on 3 days between 23 and 27 September 2009. The flights took off from Oostende in Belgium, flew with a large arc into open sea before refuelling in Rotterdam harbour, and then following the same flight pattern on the way back to measure as many ships as possible. To identify ships the helicopter hovered close to the ship while the name and IMO number was documented by hand, and Lloyds ship register was later used to retrieve DWT, DOB and ship type. The helicopter flight system was used to record the speed and heading of the ship by flying with the same speed and heading, in addition to providing the own speed, heading and altitude. Most of the wind data used was obtained from measurements in the helicopter based on comparing the true movement relative to ground to the heading of the aircraft and measured airspeed. Wind data were also obtained from a wind sensor in the North Sea (Vlaamse bank, 51.38° N, 2.43° E) and a wind mast at Hoek van Holland (51.99° N, 4.1° E).The spectrometer was located behind the pilots and the telescope was mounted on a tripod standing inside of the right passenger door. The measurement setup is shown in Fig. 8. The door had to be fully open during measurements. The flight speed

Table 1. Optical SO_2 measurements of ship emission rates performed on the Baltic sea outside Gotland on 5 days between 13 and 24 August 2008. The acronyms in the header correspond to IMO number of ship, Dead Weight Ton (DWT), ship speed in knots (v), mean SO_2 emission (E) in kg h^{-1}, and 1-σ emission variability (STD) in %.

Ship name	IMO	Ship type	DWT	v	E	Std
Sten Aurora	9318565	OIL/CHEMICAL TANKER	16.59	13.3	8	
SCF Yenisei	9333412	OIL PRODUCTS TANKER	47.18	15.1	33	26
Superfast VII	9198941	FERRY	5.915	22.8	102	24
Isabella	9255672	OIL PRODUCTS TANKER	89.99	13.3	43	11
Baltic Meridian	7710927	REEFER	9.728	17.5	57	
Finnpulp	9212644	RO-RO CARGO	10.3	16.2	48	27
Liteyny Prospect	9256078	OIL PRODUCTS TANKER	104.70	14.3	44	19
Pulpca	9345386	RO-RO CARGO	17.5	20.8	111	
Birka Carrier	9132002	RO-RO CARGO	8.853	16.3	92	
Finnmaid	9319466	FERRY	9.653	23.6	133	24
Merchant	8020604	RO-RO CARGO	13.09	16.2	37	
Timca	9307358	RORO/CONTAINER	18.25	20	77	18
Cartagena	9123817	CONTAINER SHIP	5.218	14.7	8	5
Rusich-5	9353046	CARGO	5.485	9.5	10	
Minerva Astra	9230098	CRUDE OIL TANKER	105.94	12.9	36	
Eagle Turin	9360465	CRUDE OIL TANKER	107.12	12.5	53	
Navigator II	9057458	BULK CARRIER	69.174	11.5	42	
Superfast VII	9198941	FERRY	5.915	22.7	62	21
Snow Land	7203223	REEFER	15.588	17	45	6
Pirita	9108063	CONTAINER SHIP	7.946	17.6	34	
Seabourn Pride	8707343	PASSENGERS SHIP	800	14.6	42	31
Petersburg	8311883	RO-RO CARGO	8.036	15.7	76	

Fig. 8. Measurement setup in a Dauphin helicopter used in the North Sea campaign. The picture shows the telescope with a video camera for documentation on the side. The aluminium box in the bottom right of the picture contains the spectrometer. The other boxes contain in situ gas analysers. The same system was used in the CASA-212 airplane in the Baltic Sea.

during the measurements was 36 to 137 knots and mainly around 70 knots (i.e. 35 m s^{-1}) and the altitude varied between 450 and 800 feet with most of the measurements done at 500 feet (i.e. 150 m). During the Rotterdam campaign onboard measurements were carried out on a Ro-Pax ferry, and these data have been compared to the optical measurements (see Sect. 6).

5 Results

During the Baltic Sea campaign 32 individual ships were measured with a total of 74 measurements; several ships were evaluated from multiple emission measurements. Tables 1 and 2 show the results of these measurements along with additional information about the ships. The average emissions of the measured ships are (54 ± 13) kg h^{-1} and (33 ± 8) kg h^{-1} for SO_2 and NO_2, respectively.

In the North Sea campaign 86 emission measurements of 20 ships were made. In Table 3 a selection of ships measured are shown. Figure 9 shows the histogram of the individual SO_2 measurements, with an average emission corresponding to 42 ± 11 kg h^{-1}. The detection limit of the system was sufficient to detect SO_2 in the ship plumes in 60 % of the measurements.

The average SO_2 emission per ship was lower in the North Sea campaign than in the Baltic Sea campaign. This could partly be due to the fact that a larger number of small ships were measured in the former campaign, as can be seen in the histogram in Fig. 9, but the results from the in situ measurements also indicate higher SFCs in the Baltic Sea (Mellqvist and Berg, 2012).

Table 2. Optical SO_2 measurements of ship emission rates performed on the Baltic sea outside Gotland on 5 days between 13 and 24 August 2008. The acronyms in the header correspond to IMO number of ship, Dead Weight Ton (DWT), ship speed in knots (v), mean SO_2 emission (E) in kg h^{-1}, and 1-σ emission variability (STD) in %.

Ship name	IMO	Vessel type	DWT	v	E	Std
Hans Lehmann	9406702	CARGO	12	11.7	16	
Kalkvik	9371172	CARGO	7.67	13.6	22	
Gerd Knutsen	9041057	OIL PRODUCTS TANKER	146.27	10	19	41
Frosta	9334296	OIL/CHEMICAL TANKER	5.675	14.8	5	34
Aurora	8020599	RO-RO CARGO	13.09	17.3	6	36
Glacier Point	9261396	OIL/CHEMICAL TANKER	37.28	14.3	7	27
Green Atlantic	8320585	REEFER	3.75	12.1	8	
Kang Hong	9323558	BULK CARRIER	55.589	14.8	34	
Jork	9234991	CONTAINER SHIP	11.385	17.2	45	42
Scottish Star	8315994	REEFER	13.058	16.8	43	37
Beachy Head	9234094	RO-RO CARGO	10.09	21	143	8
Snow Land	7203223	REEFER	15.588	17.1	40	
Pirita	9108063	CONTAINER SHIP	7.946	17.2	42	6

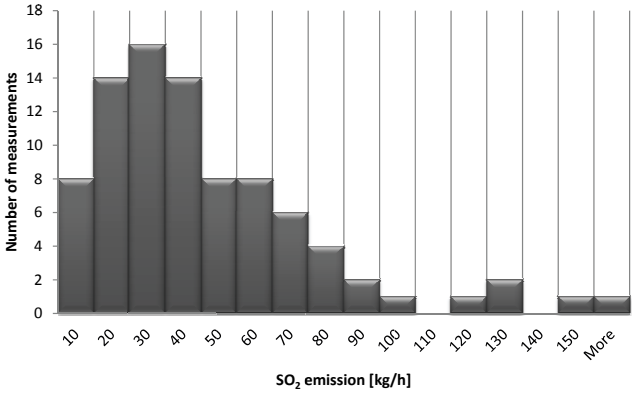

Fig. 9. Histogram of all SO_2 emission measurements by DOAS in the North Sea campaign. A relatively large number of small ships were measured close to the harbour; these were found to emit about 20 kg h^{-1} SO_2. Many of the ocean-going vessels had an emission of about 60 kg h^{-1} SO_2.

6 Discussion

6.1 Uncertainty in the optical light path

As illustrated in Fig. 5 we use a simple geometric optical path assuming the ocean to be mirror-like so that the sky light passes twice through the plume. This is however only true for wave free conditions and the mean angle of the incoming sky light, θ_{sky}, is generally different from the telescope angle, $\theta_{\text{telescope}}$. Secondly, part of the observed light is scattered directly on particles in the ship plume. To study the two upper effects properly, as a function of solar zenith angle, a 3 dimensional ray tracing model is needed which includes ocean wave scattering. This is outside the scope of this study and instead we have made a tentative error budget below, based on some simple approximations of the uncertainty sources and their potential impact.

Regarding the scattering of light in waves there are several studies (Cox and Munk, 1954; Plant, 2003; Ebuchi and Kizu, 2002) on this topic in which they have determined the mean square slope of the ocean waves and their statistical distribution under varying wind. Such information is needed for various types of remote sensing applications over the ocean. Cox and Munk (1954) did a study based on airborne photography of sun glitter assuming that the ocean was a distribution of varying angles, and that only specular reflection occurs. A distribution was found, centred at a few positive degrees with a mean square slope of 16° and a maximum slope of 35° at a wind speed of 10 m s^{-1}. In another more recent study (Ebuchi and Kizu, 2002), using several years of satellite data, a narrower distribution was found with a mean square slope of about 8° and a maximum slope of 20°.

To investigate the impact of waves on the results in our application a simplified ocean wave scattering calculation has been made approximating the ocean wave with a one dimensional sinusoidal wave, $k \cdot \sin(\phi)$. The scaling factor, k, has been chosen such that the maximum slope angle is 25°, for consistency with the literature studies above. This is illustrated in Fig. 10 for incoming light being specularly reflected on different parts, ϕ_{i}, of the wave into the line of sight of the telescope, denoted by the vector $\boldsymbol{a}$ (Eq. 6). The angle of the incoming skylight, θ_{sky}, is obtained through Eq. (8) which corresponds to the two dimensional scalar product between vector $\boldsymbol{a}$ and vector $\boldsymbol{b}$, the latter corresponding to the tangent of the ocean surface. From the calculation it is clear that most of the observed reflected light comes from the side of the wave that faces the telescope since the reflected light from the backward of the wave only is able to reach the viewing telescope through multiple wave reflection. Due to the low reflectivity of the ocean we assume this can be neglected. In the

Table 3. Optical NO_2 measurements of ship emission rates performed on the Baltic Sea outside Gotland. The data were obtained on 4 days between 12 and 24 August 2008. The acronyms in the header correspond to IMO number of ship, Dead Weight Ton (DWT), ship speed in knots (v), mean NO_2 emission (E) in kg h^{-1} and 1-σ emission variability (STD) in %.

Ship name	IMO	Ship type	DWT	v	E	Std
Taurine	7613404	General Cargo Ship	4322	15	14	2
Sloman Traveller	8214401	General Cargo Ship	9793	14	24	
Lion	8501048	General Cargo Ship	40 836	15	34	10
Sporades	9035137	Crude Oil Tanker	66 895	14	27	12
Katharina B	9121869	Container Ship (Fully cellular)	5865	12	16	32
SKS Tugela	9133460	Crude Oil Tanker	10 989	16	53	21
Maersk Flanders	9186637	Ro-Ro Cargo Ship	5700	20	39	16
Frank	9204049	Chemical/Products Tanker	14895	13	17	34
Altius	9221205	Bulk Carrier	171 481	14	22	101
Gennaro Ievioli	9223851	Chemical/Products Tanker	27 859	17	30	32
Maeris Rosyth	9236987	Chemical/Products Tanker	29 999	17	36	36
Maersk Etienne	9274642	Chemical/Products Tanker	36 941	14	32	17
Ginga Tiger	9278715	Chemical/Products Tanker	25 452	16	43	43
Endeavor	9312195	Container Ship (Fully cellular)	9168	18	20	23
Deneb J	9344241	Container Ship (Fully cellular)	11 059	18	49	20
Genco Champion	9350094	General Cargo Ship	28 445	17	28	25
Cap Castillo	9374595	Container Ship (Fully cellular)	37 763	16	56	14
Hyundai Loyalty	9393319	Container Ship (Fully cellular)	95 810	23	142	31
Stena Hollandica	9419163	Passenger/Ro-Ro Ship (Vehicles)	10 670	19	71	20
Stena Hollandica	9419163	Passenger/Ro-Ro Ship (Vehicles)	10 670	22	75	19
Maas Viking	9457165	Ro-Ro Cargo Ship	11 636	22	32	13

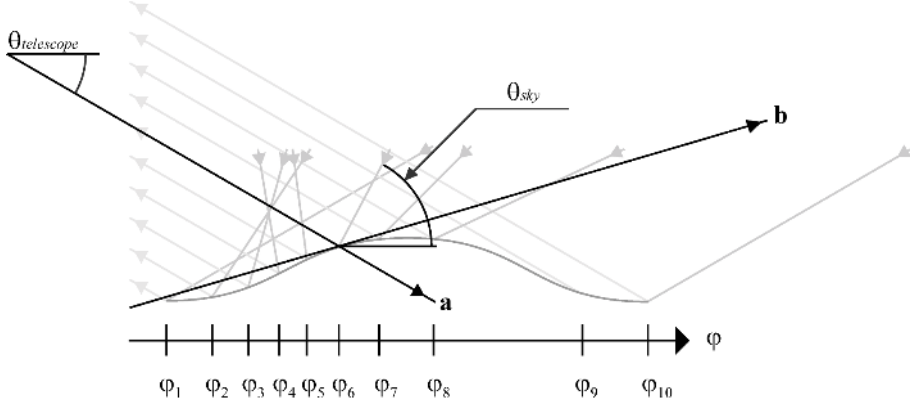

Fig. 10. Illustration of sky light scattering on a sinusoidal wave surface. Parallel rays with the angle of the telescope are used to calculate the incoming sky light angle. Vector ***a*** originates from the telescope towards the wave, at the telescope angle, and vector ***b*** is in the direction of the tangent were vector ***a*** crosses the wave. Equation (8) gives the incoming sky light angle.

calculations we calculate the average optical path from multiple θ_{sky} angles by varying the ϕ angles over several wave periods. The obtained average path corresponds to a typical θ_{sky} angle of about 50°, instead of 30°, as indicated in Fig. 5 and this leads to an airmass factor which is approximately 20 % higher according to Eq. (9). Hence for our simple case it seems that an underestimation of the measured emissions will result. It is clear that further improvements of the model is needed in the future such as two dimensional waves, presence of white caps on the waves with different reflectivity, differences between along and cross wind and taking into account the angular dependency of the reflectivity which may promote multiple reflections.

$$\boldsymbol{a} = \left[1 - \tan\left(\theta_{\text{telescope}}\right)\right] \tag{6}$$

$$\boldsymbol{b} = [1\ k\ \cos(\varphi)] \tag{7}$$

$$\theta_{\text{sky}} = 2 \cdot \text{acos}\left(\frac{\boldsymbol{a} \cdot \boldsymbol{b}}{|\boldsymbol{a}|\ |\boldsymbol{b}|}\right) - \theta_{\text{telescope}} \tag{8}$$

$$k_{\text{airmass}} = \frac{1}{\frac{1}{\sin(\theta_{\text{telescope}})} + \frac{1}{\sin(\theta_{\text{sky}})}}. \quad (9)$$

A second measurement uncertainty problem lies in the fact that part of the observed light has been scattered directly on particles in the ship plume. This is the reason why ship plumes often appear white. To study this further we have, for all ship measurements in this study, compiled the change in recorded intensity when measuring inside the plume compared to the outside. In Fig. 11 is shown a histogram of the relative intensity of the observed light in the ship plume compared to the background at the wavelength 311 nm. This is relevant for the optical SO_2 measurements. The average relative intensity here corresponds to (110 ± 20) %. At the wavelength 450 nm, relevant for the NO_2 measurement the data instead shows a relative intensity of (104 ± 10) %. There is hence more light, 4–10 % on average, when measuring through the ship plume compared to the outside, in contrast to what one would assume since both gases and particles in the ship plumes absorb light. We interpret the additional light as direct scattering of light from direct sun or diffuse sky radiation on particles in the plume. This light is redirected into the field of view of the optical telescope from various parts in the plume. A simple estimation of the effect of direct scattering is the following: assume that the ship plume is tube shaped and transparent so that multiple scattering can be neglected, and that specular reflection occurs on the water surface. Assume the measurement geometry to be such that the sun shines from behind so that the sun rays are parallel with the optical observation angle. The solar light will then be reflected into the field of view of the telescope from various positions of the gas plume. If the solar angle is similar to the observational angle it is evident that the light path of the directly scattered solar light will become shorter i.e. about half length. Assuming that 15 % of the light is directly scattered, as indicated by Fig. 11, this will cause an overestimation of the optical path length of slightly less than 10 %, and hence an underestimation in the derived emission rate. In addition to scattering of the direct solar light more than half of the incoming intensity at a given point comes from the diffuse sky radiation (Aas and Hokedal, 1999). To assess this properly we plan to run a ray trace model, for instance as published by Wagner et al. (2007). We will then also model how much of the observed light that is scattered above the gas plume. To minimize the latter effect we have flown fairly close to the plume, within 500 m.

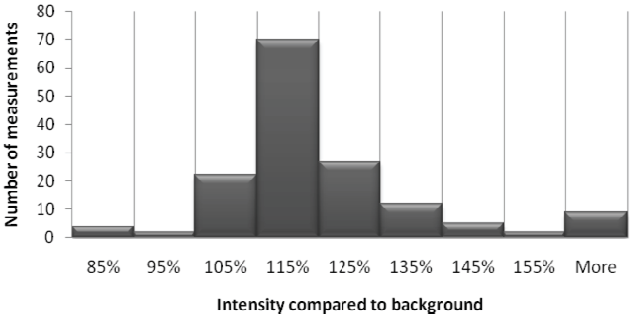

Fig. 11. Histogram of the relative intensity of the observed light in the ship plume compared to the background at the wavelength 311 nm. This is relevant for the optical SO_2 measurements.

6.2 Overall uncertainty

The random measurement uncertainty, caused by variability in the spectroscopic measurements due to noise combined with variability in the wind, has been estimated from the average variability of multiple ship measurements from the North Sea campaign and corresponds to about 20 %. For each ship we have carried out multiple measurements, typically 3, and the random uncertainty in the mean emissions is therefore reduced by the number of measurements, N.

The main systematic error when carrying out optical measurements lies in the airmass factor uncertainty due to the effect of light reflection in ocean waves and direct plume scattering, as discussed above. To assess the radiative transfer properly it is needed to carry out ray trace modelling and this is beyond the scope of this feasibility study. However, the discussion above shows tentative uncertainties of about 20 % for the influence of waves and 10 % for direct plume scattering under certain conditions, and these numbers are used for the error budget, although very uncertain.

Another large error source lies in the uncertainty in the wind speed and wind direction. Most of the used wind data has been obtained from measurements in the helicopter and aircraft. These data have been compared to other wind sensors, see Sect. 4, from which can be estimated an uncertainty of 25° in the wind direction and 1.5 m s^{-1} for the wind speed.

Other error sources includes spectroscopy and the uncertainty in the speed and heading of the target ships and the fact that the plume moves in the travel direction of the aircraft, σ'_{PM}. Another potential uncertainty is the roll angle of the aircraft/helicopter but during the flights we made certain that the airplane was balanced (not tilted) while transecting the ship plumes wherefore this error has been omitted.

In Table 5 the various uncertainties of relevance to the error budget have been compiled based on the parameters in Eq. (1). The overall uncertainty amounts to 30–45 % depending on the apparent wind speed and it is obtained as the square root sum of the squared relative uncertainties.

Regarding the uncertainty in the directional parameters of the wind and bearings of the airplane and ship we have made some simplification by neglecting these parameters when calculating the error in the apparent wind speed, this will give a maximum error. In addition is the uncertainty of the direction in the apparent wind calculated for a typical measurement, by assuming an uncertainty in the wind direction of 25°. This typically propagates as a 12° uncertainty in the

Table 4. Optical SO_2 measurements of ship emission rates performed on the North Sea. The data corresponds to 3 days between 24 and 27 September 2009. The acronyms in the header correspond to IMO number of ship, Dead Weight Ton (DWT), ship speed in knots (v), mean SO_2 emission (E) in kg h^{-1} and 1-σ emission variability (STD) in %.

Day	Time	On board kg h^{-1}	Optical kg h^{-1}	Point. dir. telescope	Light int. plume	Wind [° m^{-1} s^{-1}]	App wind [° m^{-1} s^{-1}]
25	14:58:05	100	77	Away	+6 %	294/5	106/18
25	14:59:09	100	72	Towards	+5 %	294/5	106/18
25	15:00:18	100	48	Away	+4 %	294/5	106/18
25	15:01:32	102	74	Towards	+37 %	294/5	106/18
25	15:02:31	102	70	Away	+24 %	294/5	106/18
25	15:03:37	102	94	Towards	+61 %	294/5	106/18
25	15:04:45	102	62	Away	+16 %	294/5	106/18
27	15:04:13	128	72	Away	+10 %	290/4	119/15
27	15:05:16	128	89	Towards	+21 %	290/4	119/15
27	15:06:20	128	84	Away	+16 %	290/4	119/15
27	15:07:16	128	56	Away	+4 %	290/4	119/15

apparent wind direction and furthermore as a 3 % change in the k_{ortho} factor (Eq. 5).

$$\sigma'_{\text{flux}} = \sqrt{\sigma'^2_{\text{S}} + \left(\frac{\sigma'_{\text{R}}}{\sqrt{N}}\right)^2 + \sigma'^2_{\text{L}} + \sigma'^2_{\text{AWS}} + \sigma'^2_{k_{\text{airmass}}} + \sigma'^2_{k_{\text{ortho}}}} \quad (10)$$

6.3 Validation

During the North Sea campaign the Ro-Pax ferry Stena Hollandica, on the route Rotterdam to Harwich, was used for measurement validation. From data of fuel consumption and fuel analysis data, gathered on board the ferry during the SIRENAS-R project, the sulphur emission was calculated for time periods when the optical measurements were carried out. The ferry was measured several times on two different days when leaving the Rotterdam harbour about 15 km from the shore (Table 4). Figure 12 shows the flight pattern of the Dauphin helicopter on 25 September with colour coded SO_2 columns from the optical system. On this day the emission obtained from the optical system is (30 ± 14) % lower than the emission from the onboard data. The second day, 27 September, similar measurements were carried out and the optical system now showed (41 ± 11) % lower values than the onboard emission data. The optical measurements on both of these days are similar in quality, with a precision of 20 %. In Table 4 the light increase due to direct light scattering in the plume is shown, according to the discussion in Sect. 6.1, together with the direction of the telescope relative to the ship. When measuring towards the ship the direct scattering appears more variable and for 25 September, for which there are most data, the average emission is significantly higher measuring towards the ship compared to away. For this day the columns also seems to increase as a function of increasing direct scattering with a correlation coefficient (R^2) of 0.54.

The 30–40 % lower values measured by the optical system compared to the onboard data is consistent with the tentative

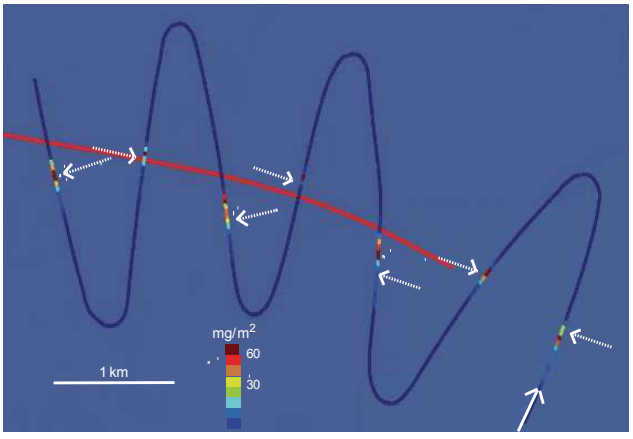

Fig. 12. An optical (DOAS) airborne measurement of the the Ro-Pax ferry Stena Hollandica at a distance of 15 km from Rotterdam harbour. The ship, displayed with the red line, is travelling eastwards in NWW wind at around 03:00 p.m. LT on 25 September. The flight path of the measuring helicopter is shown by the zigzag line with colour coded slant column values of SO_2 increasing from blue to red. The white dotted arrows indicate the direction of the incoming light observed by the DOAS and the other arrow the flight direction.

error estimation in Sect. 6.2 and the discussion of airmass factor uncertainty in Sect. 6.1 which appears to cause underestimation of the emissions values. There are however also some uncertainties regarding the on board data. The Stena Hollandica ferry has four auxiliary engines and two of these were running on low sulfur fuel with SFC of 0.5 %, to be compared with the other engines, main and auxiliary, running on a SFC of 1.4 %. We were told that the low sulphur was only used in the port but since also other types of measurements in the SIRENAS-R campaign shows lower than

Table 5. Tentative uncertainty budget for the optical emission measurement of a single ship. The shaded area corresponds to the main errors.

Abbreviation	Name	Value	Source
σ'_{S}	Spectroscopy	3 %	Literature
σ'_{R}	Random error, 3 meas.	13 %	Measured
σ'_{L}	Plume width	15 %	$\sqrt{\sigma'^2_{AS} + \sigma'^2_{PM}}$
σ'_{AWS}	Relative error in apparent wind speed	12–30 %	$\frac{1}{v_{AW}}\sqrt{\sigma^2_{WS} + \sigma^2_{SS}}$
$\sigma'_{k_{airmass}}$	Airmassfactor*	22 %	$\sqrt{\sigma'^2_{W} + \sigma'^2_{MS}}$
$\sigma'_{k_{ortho}}$	Orthogonalness of transect relative to plume	3 %	$1 - \cos\ (\sigma_{AWD})$
Total		32–43 %	
σ'_{AS}	Aircraft speed	10 %	Estimated
σ'_{PM}	Plume movement	10 %	Calculated
σ_{WS}	Wind speed	1.5 m s^{-1}	Data comparison
σ_{SS}	Ship speed	1 m s^{-1}	Calculation
v_{AW}	Apparent wind speed	6–15 m s^{-1}	Calculated
σ'_{W}	Effect of waves	20 %	Simple estimate
σ'_{MS}	Multiple scattering	10 %	Simple estimate
σ_{AWD}	Apparent wind direction (typical)	12°	Eqs. (2)–(4) and wind bearing uncertainty of 25°

* Simple approximations, rather uncertain.

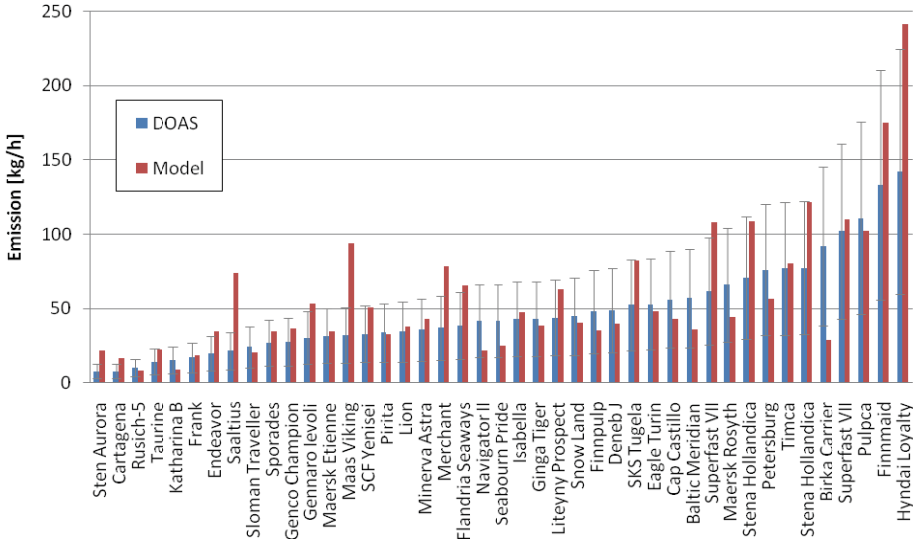

Fig. 13. Comparison of SO_2 emission rates obtained by optical measurements (DOAS) and the FMI-Steam model, for ships on the Baltic and North Sea during 2008 and 2009, respectively. The measurement error bars correspond to 40 % uncertainty.

expected values (Mellqvist and Berg, 2012) there is still some concern about this.

6.4 SO_2 and NO_x emissions versus modelled ship emissions

A ship emission model, FMI-STEAM, has been applied in this study by Jalkanen et al. (2009) to calculate sulphur and NO_x emission rates of several of the ships measured with the optical system. The model is based on the messages provided by the Automatic Identification System (AIS), carried by ships larger than 300 t, which enable the identification and location determination of ships. The use of the AIS data enables the positioning of ship emissions with a high spatial resolution. The emissions are computed based on the relationship of the instantaneous speed to the design speed, and these computations also take into account the detailed technical information of the ship engines. The modelling of emissions is also based on a few basic equations of ship design,

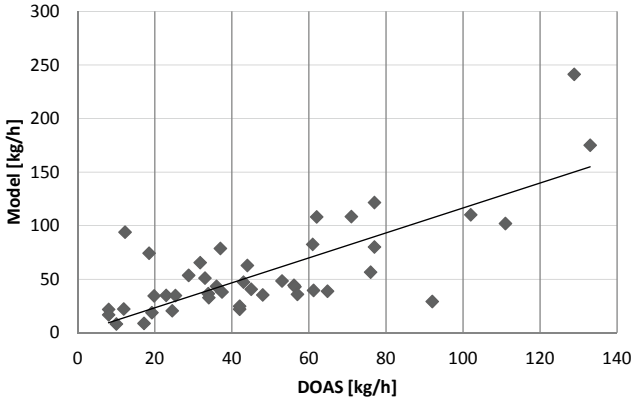

Fig. 14. Emisson rates of SO_2 from the FMI-STEAM model versus optical mearurements. The model overestimates the emissions by 18 % and the correlation coefficient (R^2) corresponds to 0.63.

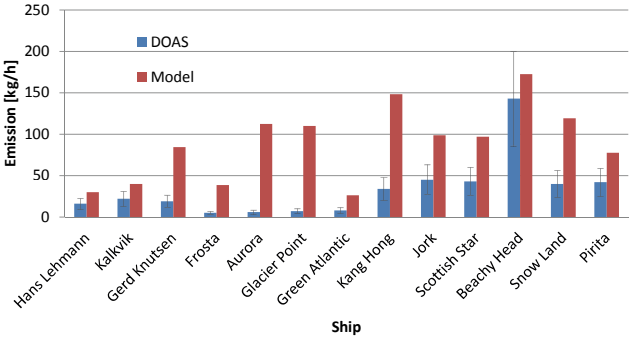

Fig. 15. Comparison of NO_2 and NO_x emission rates obtained by optical measurements (DOAS) and the FMI-Steam model, respectively, for ships on the Baltic Sea during 2008. The measurement error bars correspond to 40 % uncertainty.

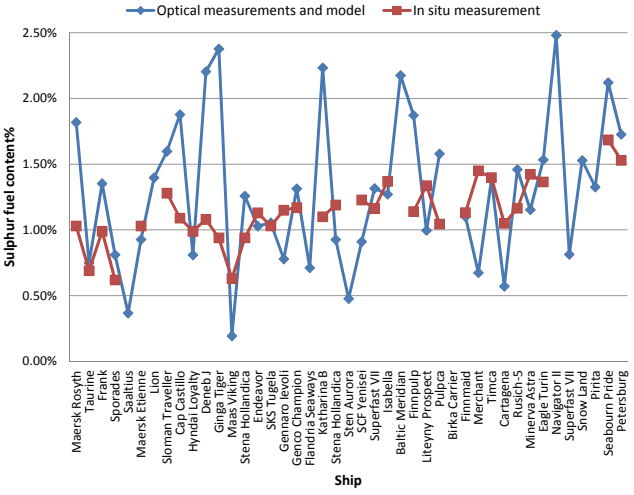

Fig. 16. Sulphur fuel content obtained by combining the optical SO_2 emission measurement with modelled power consumption and in situ measurements of SFC by conventional technique. The data correspond to ships measured on the Baltic and North Sea during 2008 and 2009, respectively.

including the modelling of the propelling power of each vessel in terms of its speed.

For the ships in this study the model assumes 1.5 % SFC for the main engines and 0.5 % for the auxiliaries. In Figs. 13 and 14 the modelling results of the SO_2 emissions for specific ships, measured in both the North Sea and Baltic Sea campaign, are compared to the optical DOAS measurements. The uncertainty bars of the optical measurements are also shown and in the SO_2 comparison most ships actually seem to be within the measurement uncertainty. In the correlation plot in Fig. 14 the model shows 18 % higher emissions than the DOAS measurements and the correlation coefficient (R^2) corresponds to 0.63.

In Fig. 15 the optical NO_2 measurements are compared with modelled NO_x emissions. Since most of the emissions actually are emitted to the air as NO the model and measured data shows rather large differences. One ship, Beachy Head, is however quite close to the model in comparison to the vessels named Jork and Scottish Star. The Beachy Head was measured from a greater distance, than the other two ships (Fig. 3), and this is consistent with the conversion of NO to NO_2 over time.

As discussed in Sect. 1, there is IMO legislation on the SFC with a 1 % maximum value on the Baltic Sea at the present that will be lowered to 0.1 % in 2015. It is therefore of large interest to carry out surveillance of individual ships to enforce the new legislation. Such surveillance is not possible to carry out directly with the optical system since the emission in $g\,s^{-1}$ is measured rather than the relative amount of sulphur in the fuel. Nevertheless it may be possible to combine the optical measurements with a model that estimates the fuel consumption to derive the SFC of the individual ships. In Fig. 16 the optical emission measurements of SO_2 have been ratioed with the modelled fuel consumption from the FMI-STEAM to yield the relative SFC. These data are compared to actual in situ measurements obtained during the SIRENAS-R campaign (Mellqvist and Berg, 2012) as briefly described in section 1. The in situ measurements are based on measuring the ratio of SO_2 and CO_2 downwind of the ships in a similar way as Williams et al. (2009). The combined optical and model data correspond to a SFC of (1.3 ± 0.5) % while the in situ data shows (1.15 ± 0.2) %. It hence seems feasible that the combined optical and model method will be able to distinguish between a ship running on 1 % SFC and one running on 0.1 %.

7 Conclusions and outlook

The DOAS method has been applied for the first time for measuring gas emissions from a ship by airborne measurements of sea scattered solar light. The result shows that the sensitivity is sufficient to detect SO_2 and NO_2 in the ship plume for a 1 s observation time. For SO_2 it was possible to detect ship plumes in 60 % of the measurements while for NO_2 the statistics are too limited.

The paper also describes a new methodology how to obtain gas fluxes from a travelling ship by optical measurements from the air. The feasibility of measuring the total SO_2 and NO_2 emission from ships in g/s has been confirmed. In a validation exercise the measurements were within 30–41 % to onboard data and this is consistent with a tentative uncertainty budget (30–45 %). For a more reliable uncertainty further modelling work is needed to estimate the optical path of the light taking into account multiple scattering in the plume and the effect of ocean waves on the effective light path through the plume.

The measurements are reasonably close to the model data in most cases for SO_2 but not for NO_2, since most of the NO_x actually is emitted as NO. By combining the optical method with calculated fuel consumption data from a ship emission model it seems feasible to distinguish between ships running with 1 % SFC versus 0.1 %; this is very interesting for the use of the method for enforcing new environmental legislation within the IMO.

Acknowledgements. The Swedish funding body Vinnova is acknowledged for financial support for the development of the IGPS measurement system and for carrying out the Baltic Sea campaign through the projects IGPS-2005-01835 and IGPS-plius-2008-03884. We thank the EU commission through DG environment for financing the SIRENAS-R campaign. The Belgian DG environment (Directorate-general Environment of the Federal Public Service Health, Food Chain Safety and Environment) is thanked for providing support for the helicopter flights as well as campaign costs in the North Sea campaign. We also acknowledge the assistance obtained from the helicopter provider NHV. We thank the Swedish Coastguard for providing the CASA-212 airplane and thank the personnel for their cooperation and project support.

Edited by: A. Richter

References

Aas, E. and Hökedal, J.: Reflection of Spectral Sky Irradiance on the Surface of the Sea and Related Properties, Remote Sens. Environ., 70, 181–190, 1999.

Beirle, S., Platt, U., von Glasow, R., Wenig, M., and Wagner, T.: Estimate of nitrogen oxide emissions from shipping by satellite remote sensing, Geophys. Res. Lett., 31, L18102, doi:10.1029/2004gl020312, 2004.

Corbett, J. J., Winebrake, J. J., Green, E. H., Kasibhatla, P., Eyring, V., and Lauer, A.: Mortality from ship emissions: A global assessment, Environ. Sci. Technol., 41, 8512–8518, doi:10.1021/Es071686z, 2007.

Cox, C. and Munk, W.: Measurement of the Roughness of the Sea Surface from Photographs of the Suns Glitter, J. Opt. Soc. Am., 44, 838–850, 1954.

Ebuchi, N. and Kizu, S.: Probability distribution of surface wave slope derived using sun glitter images from Geostationary Meteorological Satellite and surface vector winds from scatterometers, J. Oceanogr., 58, 477–486, 2002.

European Commission: Thematic Strategy on air pollution, Commission of the European Communities, Brussels, Communication from the commission to the council and the European parliament COM(2005) 446 final, 2005.

Fish, D. J. and Jones, R. L.: Rotational Raman-Scattering and the Ring Effect in Zenith-Sky Spectra, Geophys. Res. Lett., 22, 811–814, 1995.

Galle, B., Oppenheimer, C., Geyer, A., McGonigle, A. J. S., Edmonds, M., and Horrocks, L.: A miniaturised ultraviolet spectrometer for remote sensing of SO2 fluxes: a new tool for volcano surveillance, J. Volcanol. Geoth. Res., 119, 241–254, 2003.

Grainger, J. F. and Ring, J.: Anomalous Fraunhofer line profiles, Nature, 193, 762, 1962.

IMO: Revised Marpol Annex VI, Regulation for the prevention of air pollution from ships and NO_x technical code 2008, 2009 Edn., IMO publishing, London, ISBN 978-92-801-4243-3, 2009.

Jalkanen, J.-P., Brink, A., Kalli, J., Pettersson, H., Kukkonen, J., and Stipa, T.: A modelling system for the exhaust emissions of marine traffic and its application in the Baltic Sea area, Atmos. Chem. Phys., 9, 9209–9223, doi:10.5194/acp-9-9209-2009, 2009.

Johnson, J. E., Tarrasón, L., and Bartnicki, J.: Effects of international shipping on European pollution levels, EMEP MSC-W Report 2000, ISSN 0332-9879, 2000.

Kraus, S.: DOASIS A Framework Design for DOAS, Shaker Verlag, 2006.

Lee, C., Richter, A., Weber, M., and Burrows, J. P.: SO_2 Retrieval from SCIAMACHY using the Weighting Function DOAS (WF-DOAS) technique: comparison with Standard DOAS retrieval, Atmos. Chem. Phys., 8, 6137–6145, doi:10.5194/acp-8-6137-2008, 2008.

Mellqvist, J. and Berg, N.: Airborne surveillance of sulphur and NO_x in ships as a tool to enforce IMO legislation, Atmos. Meas. Tech., in preparation, 2012.

Mellqvist, J., Samuelsson, J., Johansson, J., Rivera, C., Lefer, B., Alvarez, S., and Jolly, J.: Measurements of industrial emissions of alkenes in Texas using the solar occultation flux method, J. Geophys. Res.-Atmos., 115, D00f17, doi:10.1029/2008jd011682, 2010.

Plant, W. J.: A new interpretation of sea-surface slope probability density functions, J. Geophys. Res.-Oceans, 108, 3295, doi:10.1029/2003jc001870, 2003.

Platt, U., Perner, D., and Pätz, H. W.: Simultaneous Measurement of Atmospheric CH_2O, O_3 and NO_2 by Differential Optical Absorption, J. Geophys. Res., 84, 6329–6335, 1979.

Rivera, C., Sosa, G., Wöhrnschimmel, H., de Foy, B., Johansson, M., and Galle, B.: Tula industrial complex (Mexico) emissions of SO_2 and NO_2 during the MCMA 2006 field campaign using a mobile mini-DOAS system, Atmos. Chem. Phys., 9, 6351–6361, doi:10.5194/acp-9-6351-2009, 2009.

Van Roozendael, M. and Fayt, C.: WinDOAS 2.1 Software User Manual, Bira-IASB, Brussels, 2001.

Vandaele, A. C., Hermans, C., Simon, P. C., Carleer, M., Colin, R., Fally, S., Merienne, M. F., Jenouvrier, A., and Coquart, B.: Measurements of the NO_2 absorption cross-section from $42\,000\,cm^{-1}$ to $10\,000\,cm^{-1}$ (238–1000 nm) at 220 K and 294 K, J. Quant. Spectrosc. Ra., 59, 171–184, 1998.

Wagner, T., Burrows, J. P., Deutschmann, T., Dix, B., von Friedeburg, C., Frieß, U., Hendrick, F., Heue, K.-P., Irie, H., Iwabuchi, H., Kanaya, Y., Keller, J., McLinden, C. A., Oetjen, H., Palazzi, E., Petritoli, A., Platt, U., Postylyakov, O., Pukite, J., Richter, A., van Roozendael, M., Rozanov, A., Rozanov, V., Sinreich, R., Sanghavi, S., and Wittrock, F.: Comparison of box-air-mass-factors and radiances for Multiple-Axis Differential Optical Absorption Spectroscopy (MAX-DOAS) geometries calculated from different UV/visible radiative transfer models, Atmos. Chem. Phys., 7, 1809–1833, doi:10.5194/acp-7-1809-2007, 2007.

Wang, P., Richter, A., Bruns, M., Burrows, J. P., Scheele, R., Junkermann, W., Heue, K.-P., Wagner, T., Platt, U., and Pundt, I.: Airborne multi-axis DOAS measurements of tropospheric SO_2 plumes in the Po-valley, Italy, Atmos. Chem. Phys., 6, 329–338, doi:10.5194/acp-6-329-2006, 2006.

Williams, E. J., Lerner, B. M., Murphy, P. C., Herndon, S. C., and Zahniser, M. S.: Emissions of NO_x, SO_2, CO, and HCHO from commercial marine shipping during Texas Air Quality Study (TexAQS) 2006, J. Geophys. Res., 114, D21306, doi:10.1029/2009JD012094, 2009.

Yu, Y., Panday, A., Hodson, E., Galle, B., and Prinn, R.: Monocyclic aromatic hydrocarbons in Kathmandu during the winter season, Water Air Soil Poll., 191, 71–81, doi:10.1007/s11270-007-9607-6, 2008.